Diminished cortical excitation during perceptual impairments in a mouse model of autism

Joseph Del Rosario[1], Anderson Speed[1], Hayley Arrowood[1], Cara Motz[1,2], Machelle Pardue[1,2], Bilal Haider[1,*]

[1] Biomedical Engineering, Georgia Institute of Technology & Emory University, Atlanta, USA

[2] Atlanta VA Center for Visual and Neurocognitive Rehabilitation, Decatur, USA

*Lead contact: bilal.haider@bme.gatech.edu

Abstract

Sensory impairments are a core feature of autism spectrum disorder (ASD). These impairments affect visual perception (Robertson and Baron-Cohen, 2017), and have been hypothesized to arise from imbalances in excitatory and inhibitory activity in cortical circuits (Rubenstein and Merzenich, 2003; Nelson and Valakh, 2015; Sohal and Rubenstein, 2019); however, there is little direct evidence testing this hypothesis in identified excitatory and inhibitory neurons during relevant impairments of sensory perception. Several recent studies have exploited transgenic mouse models of ASD to examine excitatory and inhibitory activity in ASD (Goel et al., 2018; Antoine et al., 2019; Lazaro et al., 2019), but have provided conflicting accounts for the relative importance of excitatory versus inhibitory activity underlying sensory deficits. Here, we utilized a genetically relevant mouse model of ASD (CNTNAP2$^{-/-}$; Arking et al., 2008; Penagarikano et al., 2011) and directly measured excitatory and inhibitory neural circuit activity in primary visual cortex (V1), while measuring visual perceptual behavior (Speed et al., 2019). We found that ASD mice showed quantitative impairments in the speed and accuracy of visual perception, and these impairments were simultaneously associated with diminished excitatory neuron activity and aberrant low frequency network oscillations in superficial cortical layers 2/3 (L2/3). These results establish that perceptual deficits associated with ASD can arise from reduced sensory excitation rather than elevated inhibition in cortical circuits.

Introduction

Impaired sensory perception is a key feature of autism spectrum disorder (ASD) (Robertson and Baron-Cohen, 2017). Sensory disturbances may occur in >90% of individuals with ASD (Tavassoli et al., 2014), and are present early in development (Tomchek and Dunn, 2007). These sensory symptoms can predict later disease severity (Estes et al., 2015). Since there is detailed knowledge about the neural circuit basis of mammalian sensory processing, understanding impaired sensory perception in autism models provides an entry point for identifying neural circuit dysfunctions underlying core symptoms of ASD.

A prominent theory of ASD proposes that imbalanced excitatory-inhibitory activity ratios in cortex generate behavioral deficits (Rubenstein and Merzenich, 2003; Nelson and Valakh, 2015; Sohal and Rubenstein, 2019). However, little direct evidence for this hypothesis has been measured from identified excitatory and inhibitory neurons during quantifiable behavioral impairments. One recent study found that inhibitory neurons are more perturbed than excitatory neurons in superficial cortical layers 2/3 (L2/3) in a Fragile X syndrome mouse model of ASD (Goel et al., 2018). However, another study observed reduced and poorly coordinated excitatory activity in frontal cortex of the CNTNAP2$^{-/-}$ ASD mouse model (Lazaro et al., 2019), but these excitatory activity deficits were not measured during sensory impairments or behavior. A third study suggests that these and multiple other ASD models internally compensate for deficits of excitatory and inhibitory activity,

resulting in overall preserved sensory responsiveness (Antoine et al., 2019); crucially, this study also did not measure neural activity deficits during sensory perceptual impairments. It thus remains unresolved if excitatory or inhibitory neural activity deficits underlie simultaneous perceptual impairments in ASD mouse models.

There is extensive mechanistic knowledge about the excitatory and inhibitory basis of visual processing (Douglas and Martin, 2004; Isaacson and Scanziani, 2011; Priebe and Ferster, 2012; Haider et al., 2013), providing an ideal framework for resolving questions about neural activity deficits and perceptual impairments in ASD. Remarkably, deficits of visual processing arise as early as primary visual cortex (V1) in individuals with ASD (Robertson et al., 2014). We recently established that the state of cortical activity in V1 plays a decisive role for trial-by-trial visual spatial perception in mice (Speed et al., 2019). This platform enabled us to directly measure excitatory and inhibitory neural circuit activity in V1 of CNTNAP2$^{-/-}$ ASD model mice while measuring the speed and accuracy of perceptual behavior. We found that ASD mice showed quantitative deficits in visual perception, and these were associated with diminished excitatory neuron activity and aberrant low frequency network oscillations in the superficial layers of V1.

Results

We trained both C57BL6J (wildtype, WT) and CNTNAP2$^{-/-}$ autism spectrum disorder (ASD) model mice to report perception of spatially localized visual stimuli. Mice learned to lick for water rewards when visual stimuli (horizontally oriented Gabor gratings, see Methods) appeared on a screen (Fig. 1A). Stimuli appeared only after a mandatory period of no licking (0.5 – 6 s, randomized per trial), and rewards were delivered only upon the first lick during the stimulus response window (typically 1 – 1.5 s). We quantified perceptual performance using signal detection theory (Green and Swets, 1974). Our prior studies in WT mice showed that detection of stimuli in the peripheral (monocular) visual field is more difficult than detection in the central (binocular) visual field. (Speed et al., 2019). Here we found that ASD mice had lower detection sensitivity than WT mice for stimuli appearing in these more difficult (monocular) spatial locations (Extended data Fig. 1-1). Since the goal of our study was to examine neural activity deficits in ASD mice during repeatable and robust measurements of perceptual performance, here we focused on examining neural correlates of binocular visual detection. This allowed us to measure large numbers of correct and incorrect behavioral trials, while presenting visual stimuli at the same spatial locations, visual contrasts, and durations for both WT and ASD mice (see Methods).

ASD mice detected binocular visual stimuli more slowly and less accurately than WT mice. ASD mice showed significantly slower reaction times (Fig. 1B-C), and significantly fewer correct (Hit) trials of stimulus detection (Fig. 1D) than WT mice. However, ASD mice also made fewer false alarms, which overall led to psychometric detection sensitivity (d') that did not differ significantly from WT mice (Fig. 1E-F, see Methods). These measurements also revealed that ASD mice held a significantly more conservative response bias than WTs (Fig. 1G). However, this conservative response bias was not simply explained by lower arousal—in fact, ASD mice showed higher arousal (measured via pupil area) than WT mice before stimulus onset (Extended data Fig. 1-2), and both WT and ASD mice showed relatively lower arousal preceding correct detection, consistent with prior reports (McGinley et al., 2015; Speed et al., 2019). Moreover, response vigor was comparable for ASD and WT mice on Hit trials (similar licking frequencies, one fewer lick per reward in ASD mice, Extended data Fig. 1-2), arguing against gross motor deficits as a main factor for perceptual impairments. Importantly, perceptual impairments were also not

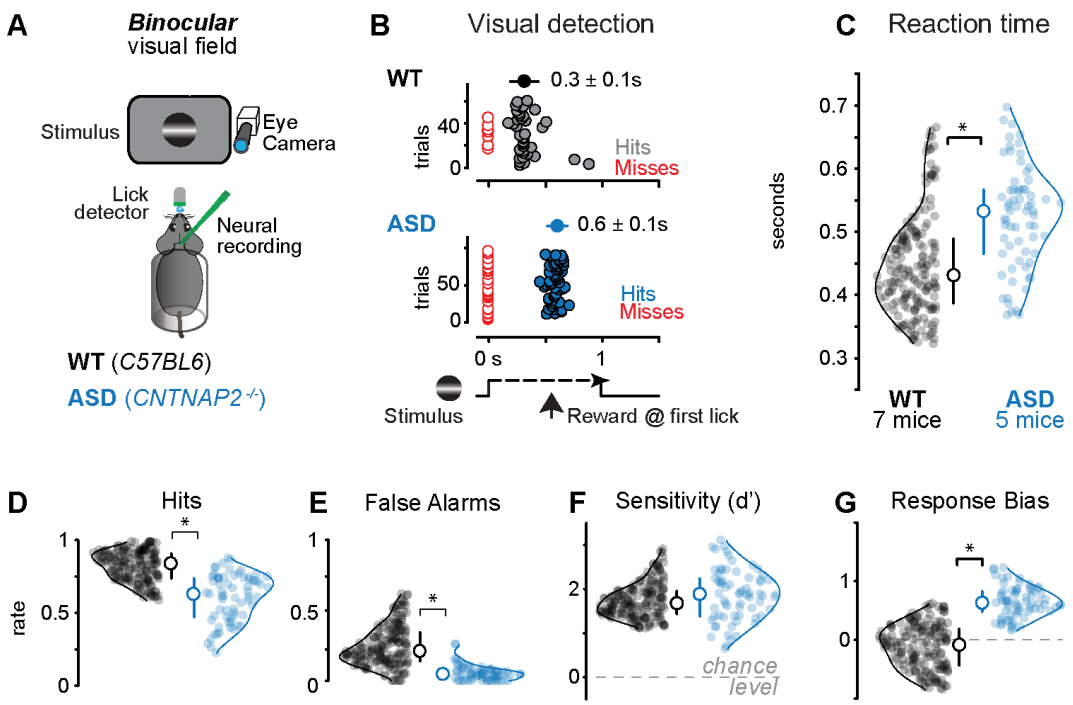

Figure 1. Visual perceptual behavior is impaired in a mouse model of ASD

A. Head-fixed mice were trained to detect visual stimuli in the binocular visual field by licking to obtain water reward. Pupil activity, neural activity, and licking was recorded simultaneously with behavior. C57BL6J (Wildtype, WT) in black, CNTNAP2$^{-/-}$ (ASD) in blue throughout.

B. Example behavioral session shows detection latency (reaction time) was markedly slower for ASD versus WT mice. Stimulus time course shown at bottom, with first lick times on correct trials (hits, colored circles) shown for individual consecutive trials (ordinate). Failures of detection (Misses) plotted in red. Average reaction times: WT, 0.3 ± 0.1s; ASD, 0.6 ± 0.1s, mean ± SD reported throughout the figure.

C. ASD mice detected stimuli significantly more slowly than WT mice (ASD: 0.52 ± 0.08, 71 sessions, 7 mice; WT: 0.45 ± 0.08, 187 sessions, 5 mice; $p < 0.01$). Average stimulus contrast was similar across ASD and WT mice (WT: 23 ± 24%; ASD: 23 ± 22%). Circles show reaction time average per session. Median ± IQR plotted inside the distributions.

D. ASD mice showed significantly lower hit rates (ASD: 0.6 ± 0.18; WT: 0.82 ± 0.12; $p < 0.01$).

E. ASD mice showed significantly lower false alarm rates (ASD: 0.06 ± 0.07; WT: 0.24 ± 0.15; $p < 0.01$).

F. Sensitivity index (d') was not different between ASD and WT mice (ASD: 1.84 ± 0.71; WT: 1.74 ± 0.47; $p = 0.1$).

G. ASD mice showed higher criterion (c) indicating increased bias to withhold from responding (WT: 0.12 ± 0.43; ASD: 0.65 ± 0.29; $p < 0.01$). Criterion was significantly greater than 0 for ASD mice, but not for WT mice (WT: $p = 0.06$; ASD: $p < 0.01$). C – G all during same behavioral trials.

explainable by slower or reduced visual responses in the retina—these were nearly identical in ASD and WT mice across a wide range of light intensities (Extended data Fig. 1-3).

ASD mice displayed weaker excitatory sensory processing in V1, but only during wakefulness. We first measured fast spiking (FS, putative inhibitory) and regular spiking (RS, putative excitatory) neuron populations (Extended data Fig. 2-1) with silicon probe recordings across layers of V1 during

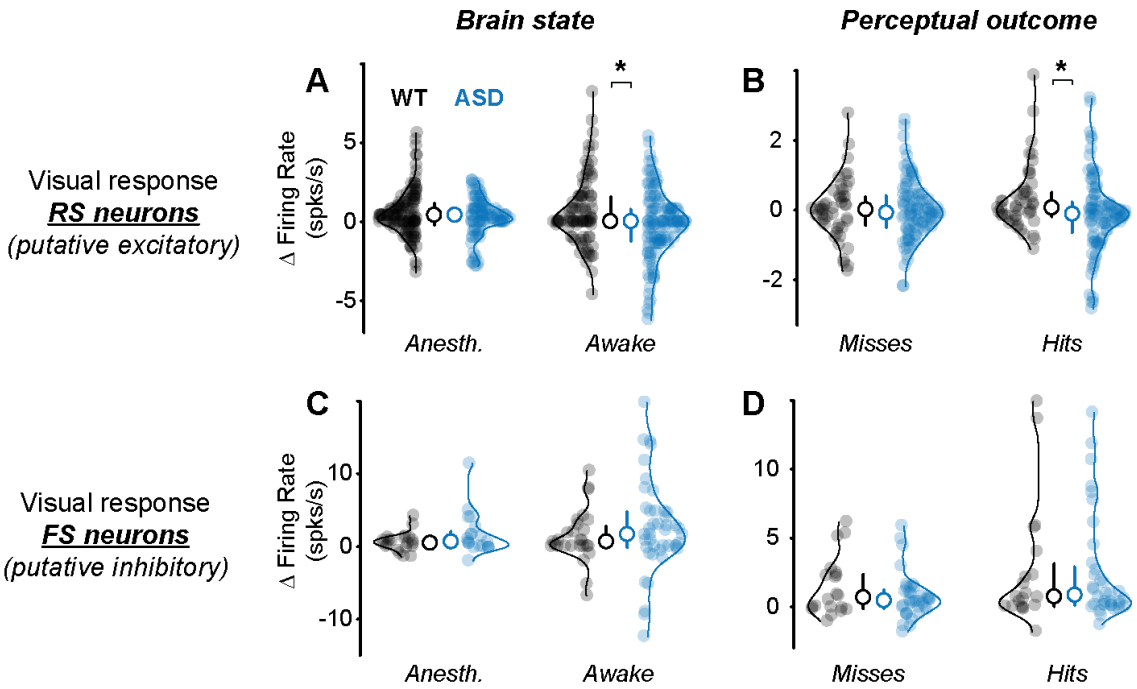

Figure 2. Visual responses of excitatory but not inhibitory neurons are diminished in ASD mice

A. Visual responses to high contrast bars in regular spiking (RS) putative excitatory neurons. Left, no significant difference during anesthesia (WT: Δ0.59 ± 0.17 spikes / s, mean ± SEM reported throughout figure, n = 129 neurons; ASD: Δ0.24 ± 0.14, n = 96 neurons; *p=0.29*, single-tail rank sum test). Right, responses in ASD mice were significantly reduced during wakefulness (WT: Δ0.72 ± 0.33 spikes / s, n = 95 neurons; ASD: Δ-0.22 ± 0.24, n = 131 neurons; *p<0.05*, single-tail rank sum test). Median and IQR plotted inside distributions. ΔResponse calculated as difference between pre- and post-stimulus activity (see Methods).

B. During perceptual behavior, RS activity was significantly reduced in ASD mice selectively on correct detection (Hit) trials (WT: Δ0.45 ± 0.25 spikes / s, n = 49 neurons; ASD: Δ–0.10 ± 0.14, n = 103 neurons; *p < 0.05*, single-tail rank sum test). Activity was not different during Miss trials (WT: Δ0.09 ± 0.1 spikes / s; ASD: Δ0.02 ± 0.11, *p = 0.22*, single-tail rank sum test).

C. No significant difference in fast spiking (FS) putative inhibitory neuron responses during anesthesia (WT: Δ0.66 ± 0.33 spikes / s; n = 23 neurons; ASD: Δ1.84 ± 0.84, n = 22 neurons; *p=0.55*, single-tail rank sum test) or wakefulness (WT: Δ1.61 ± 0.95 spikes / s; n = 45 neurons; ASD: Δ2.44 ± 1.09, n = 29 neurons; *p=0.21,* single-tail rank sum test).

D. No significant difference in FS activity on Hit trials (WT: Δ2.58 ± 0.10 spikes / s, n = 20 neurons; ASD: Δ2.88 ± 0.84, n = 38 neurons; *p=0.78*, single-tail rank sum test) or Miss trials (WT: Δ1.40 ± 0.47 spikes / s; ASD: Δ0.81 ± 0.34; *p=0.43*, single-tail rank sum test).

anesthesia; here we observed no differences in the overall distributions of visually-evoked spiking in either RS or FS neurons of ASD versus WT mice (Fig. 2A, C). In contrast, recordings during wakefulness (in the absence of the behavioral task) revealed that visually-evoked spiking of RS neurons in ASD mice was significantly reduced versus WTs, but with no differences in FS neuron responses during the same recordings (Fig. 2A, C). Reduced excitatory responsiveness was not explained by smaller receptive fields in ASD mice (Extended data Fig. 2-2), nor by shorter latency or duration of neural responses in ASD mice during anesthesia or wakefulness (Extended data Figs. 2-1, 2-3).

ASD mice also showed reduced RS neuron activity during perceptual behavior. Recordings in binocular V1 (Extended data Fig. 2-1) revealed fewer visually-evoked spikes in RS neurons of ASD mice on correct binocular detection (Hit) trials (Fig. 2B). These activity deficits were not apparent on incorrect detection (Miss) trials and were not apparent in FS neurons (Fig. 2D). Again, these results were not explainable by slower neural response latencies in ASD mice at these same recording sites, either at the level of local field potential (LFP, Extended data Fig. 2-4), or visually-evoked spiking (Extended data Fig. 2-5). If anything, ASD neural responses were slightly faster than WTs, consistent with prior findings (Bertone et al., 2005). We also examined trial-to-trial variability in both LFP and spiking responses, but this was comparable in WT versus ASD mice and did not explain behavioral differences (not shown here).

These deficits in excitatory neuron activity in ASD mice were most pronounced in Layer 2/3 (L2/3). We identified cortical layers in V1 using current source density analysis (Extended data Fig. 2-1), and assigned neural activity to L4, L2/3, and L5/6. Strikingly, we isolated fewer neurons in L2/3 of ASD mice versus WT mice during behavioral recordings, even though recording quality across days was comparable (Extended data Fig. 3-1); moreover, the isolation of neurons in ASD mice was not uniformly reduced in other layers (Extended data Fig. 3-1). The lower fraction of active and isolatable L2/3 RS neurons during behavior suggested that overall activity levels were lower in L2/3 of ASD mice (Fig. 3A). Consistent with these observations, multi-unit (MU) activity was also reduced in L2/3 of ASD mice (not shown), and peak-to-peak amplitudes for visually-evoked LFP in L2/3 were also significantly smaller in ASD versus WT mice (Extended data Fig. 3-2), while LFP amplitudes in other layers were unaffected. We thus aggregated across all awake recordings (both inside and outside of the behavioral task) and found that L2/3 excitatory neurons in ASD mice showed significantly smaller action potential waveforms versus WT mice (Fig. 3B). Importantly, in these same recordings, RS and FS neurons in L4 and L5/6 did not show significant differences in action potential amplitudes or activity profiles during behavior (L4: FS, $p=0.27$; RS, $p = 0.35$; L5/6: FS, $p=0.29$, RS, $p = 0.12$; rank sum tests).

During perceptual behavior, L2/3 LFP in ASD mice displayed aberrant low frequency power, and this degraded the relationship of neural activity to perceptual performance. We and others have recently shown that elevated low frequency (3 – 7 Hz) LFP power in V1 correlates with and predicts failures of stimulus detection in WT mice (Einstein et al., 2017; Speed et al., 2019). Remarkably, in ASD mice 3 – 7 Hz LFP power was significantly elevated on both correct and incorrect detection trials (Fig. 3C). Consequently, the difference in low frequency power on correct versus incorrect trials was less separable in ASD mice (Fig. 3D). Consistent with our previous results, single-trial perceptual outcomes were accurately predicted from the 3 – 7 Hz LFP power in WT mice; however, perceptual outcome predictions from L2/3 LFP were significantly worse in ASD mice (Fig. 3E). Moreover, in WT mice L2/3 LFP power was strongly correlated with reaction time on correct trials (Fig. 3F); in contrast, the relationship between L2/3 LFP power and reaction times in ASD mice was nearly flat. These results link excitatory neural activity deficits in L2/3 of ASD mice to simultaneous impairments in both the speed and accuracy of visual perception.

Discussion

Here we showed that diminished excitatory signaling in cortex accompanies impaired sensory perception in the human-relevant CNTNAP2$^{-/-}$ transgenic mouse model of autism spectrum disorder (ASD). Using a well-controlled, head-fixed visual detection task, we quantified perceptual performance while recording V1 neural activity driven by

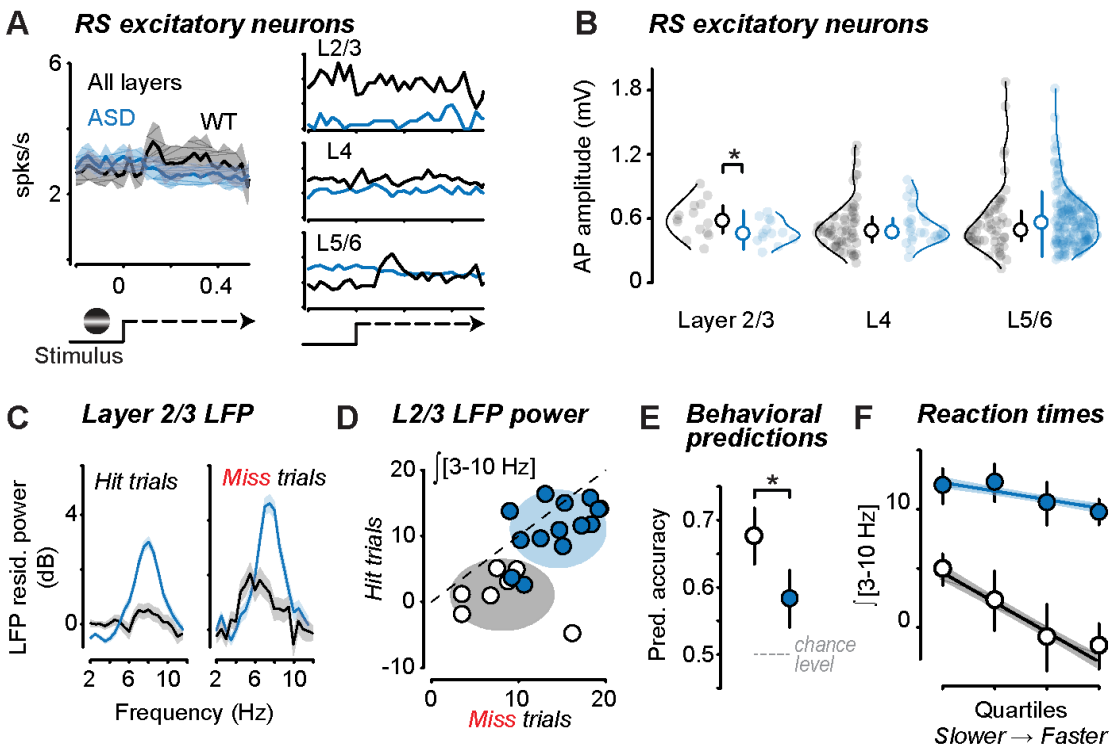

Figure 3. Excitatory activity deficits in L2/3 impair perceptual performance in ASD mice

A. Peristimulus time histograms (PSTHs) of average RS activity across all layers (left) and split by layers (right) on correct detection trials.

B. Action potential amplitudes in L2/3 RS neurons in ASD mice (0.48 ± 0.03 mV; mean ± SEM n = 13) were significantly smaller than in WT mice (0.59 ± 0.04 mV, n = 14; *p<0.05*, single-tail rank sum test). There were no such differences in L4 (ASD: 0.54 ± 0.03; n = 28; WT: 0.54 ± 0.03, n = 59; *p=0.35*) or L5/6 (ASD: 0.59 ± 0.02; n = 178; WT: 0.58 ± 0.04, n = 53; *p=0.12)*. Neurons aggregated across anesthetized and awake recordings. Median ± IQR plotted inside distributions.

C. Low frequency local field potential (LFP) residual power in L2/3 is significantly elevated in ASD versus WT mice on both Hit trials (ASD: 10.99 ± 0.65, n = 1402 trials, 15 recordings in 3 mice; WT: 1.21 ± 0.97, n = 533 trials, 7 recordings in 3 mice; *p<0.01*) and Miss trials (ASD: 13.62 ± 0.98, n = 423 trials; WT: 7.33 ± 1.34, n = 211 trials; *p<0.01*). Mean ± SEM of integrated power 3 – 10 Hz. See Methods for calculation of residual power.

D. Integrated 3-10Hz residual power is greater on Misses versus Hits in both ASD and WT mice (*p<0.01* for both). Shaded regions show 2-D Gaussian fit ± 1σ.

E. Predictions of perceptual outcome from low frequency LFP power were significantly worse in ASD mice (58 ± 4% accuracy; mean ± SD; cross-validated linear classifier) versus WT mice (68 ± 4% accuracy; *p<0.01*). See Methods for classifier description.

F. Low frequency LFP residual power is significantly and negatively correlated with reaction time in WT mice (r^2=0.18; *p<0.05*, F-test), but not in ASD mice (r^2=0.03; *p=0.22*, F-test). Single trial reaction times (Hit trials) were binned into quartiles, and single trial integrated 3-10Hz LFP residual power was averaged within quartile for all WT and ASD trials (mean ± SEM). Shaded regions are bootstrap error bars (see Methods).

spatially localized sensory stimuli. ASD mice detected visual stimuli more slowly than WT mice and displayed simultaneous deficits of excitatory activity in L2/3. Population activity in L2/3 of ASD mice was strongly synchronized at low frequencies (3 – 7 Hz) across all trial types. This aberrant low frequency activity was detrimental for

predicting perceptual performance from neural activity in V1. Together, our results identify excitatory rather than inhibitory activity deficits underlying perceptual impairments in a genetically relevant mouse model of ASD.

Perceptual impairments in ASD mice manifested as both slower and less accurate detection. The latency for generating rewarded motor actions was slower in ASD versus WT mice, despite stimuli appearing at the same locations and same visual contrast ranges across experiments. These longer latency responses were not trivially explained by slower sensory signals in ASD mice: latencies in retina and L4 of V1 were nearly identical with WT mice; likewise, acuity and visual response latencies in individuals with ASD appear largely unaffected (Sutherland and Crewther, 2010; Tavassoli et al., 2011). Individuals with ASD can also show slower and less reliable perceptual reaction times (Karalunas et al., 2014), but this remains debated (van der Geest et al., 2001; Ferraro, 2016). Nonetheless, it appears that the latency of neural signals transmitted from V1 cannot easily explain slower perception. In our study, behavioral impairments were associated with and predicted by deficits in L2/3 RS neuron activity, the major source of feedforward projections to higher visual areas (Glickfeld et al., 2013). One possibility is that these feedforward visual signals are poorer quality and integrated more slowly in downstream areas. Simultaneous recordings in V1, higher visual areas, and lick-related motor areas may reveal how deficits in the amplitude and timing of sensory-motor signals lead to delayed and impaired perception in ASD.

We found that excitatory neural activity deficits in ASD mice were dependent upon brain state. Recordings of both FS inhibitory and RS excitatory neurons during anesthesia did not reveal overall differences in visually-evoked firing rates; however, recordings during wakefulness revealed reduced responses in RS excitatory neurons specific to behavioral conditions and perceptual outcomes. This suggests that the brain-wide synchronizing effects of anesthesia (Haider et al., 2013) may mask fine-scale neural activity deficits in models of ASD. This highlights the need to not only compare the properties of neural circuits across multiple models of ASD (Antoine et al., 2019), but also across multiple brain states and behavioral outcomes. Although we found that differences in arousal (as measured via pupillometry) could not explain perceptual impairments, neural activity deficits may be more pronounced with behaviorally relevant engagement of neuromodulatory systems, an important topic for future investigations.

We identified a constellation of activity deficits in excitatory neurons in superficial cortical layers during perceptual deficits in ASD mice. These deficits in excitatory neurons of L2/3 are remarkably consistent with a recent study identifying alterations specifically in excitatory neurons in superficial cortical layers of individuals with ASD (Velmeshev et al., 2019). Here, we found three major deficits in cortical L2/3 function during perceptual impairments. First, sensory-evoked excitatory firing rates were significantly lower, in a state-dependent manner. Second, action potential amplitudes in L2/3 RS neurons were significantly smaller than in WT mice, perhaps contributing to a lower incidence of well-isolated single neurons in L2/3 of ASD mice (Scott et al., 2019). Third, elevated low frequency power in L2/3 of ASD mice accompanied sensory impairments. Our previous studies in WT mice showed that these low frequencies are detrimental for visual detection, with nearly 90% of perceptual failures predicted by elevated 3 - 7 Hz LFP power (Speed et al., 2019). Here, we found that ASD mice showed significantly elevated low frequency power on all behavioral trials; this worsened the predictability of behavior from neural activity and obscured the relationship of neural activity to reaction times on correct trials. It remains to be seen if low frequency oscillations play a causal role in directly

impairing visual perception in ASD mice, or if they are a network-wide consequence of reduced activity in specific excitatory neurons. Our prior study recorded in monocular regions of V1 during monocular detection and found that these low-frequency oscillations were most prominent in L4 (Speed et al., 2019); here we recorded in binocular V1, during binocular detection trials. However, recent studies observed similar low frequency oscillations in L2/3 and these also reduced visual responsiveness of excitatory neurons in L2/3 of WT mice (Einstein et al., 2017). The laminar differences in oscillations across retinotopic areas of WT and ASD mice remain to be explored. Another recent study directly induced low-frequency oscillations in primate visual cortex, and these caused visual perceptual impairments (Nandy et al., 2019). An intriguing possibility is that low frequency oscillations in L2/3 reduce the dynamic range available to transmit feedforward sensory information to downstream areas during behavior. This suggests that directly reducing low frequency synchronization in L2/3 neurons may restore excitatory signaling bandwidth and remedy perceptual deficits in ASD, a hypothesis that now seems testable in mice.

Methods

Experimental model and subjects

All procedures were approved by the Institutional Animal Care and Use Committee at the Georgia Institute of Technology and were in agreement with guidelines established by the National Institutes of Health.

Surgery. Male C57BL6J (RRID: IMSR_JAX:000664) and CNTNAP2$^{-/-}$ (RRID: IMSR_JAX:017482) mice (5 – 8 weeks old; reverse light cycle individual housing; bred in house) were chronically implanted with a stainless steel headplate with a recording chamber during isoflurane (1-2%) anesthesia. The headplate was affixed to the skull using thin layer of veterinary glue (Vetbond) and secured using dental cement (Metabond). The recording chamber was sealed with a removable polymer (KwikCast). After implant surgery mice were allowed to recover for 3 days before experimentation. During recovery mice were habituated to experimenter handling.

Behavior

Water restriction. Following recovery from surgery, mice were placed under a restricted water schedule (to provide motivation) and trained to detect visual stimuli for water reward. Mice received a daily minimum amount of water (40 ml/kg/day; Burgess et al., 2017; Speed et al., 2019). If mice did not receive their daily minimum water in task, they received supplemental hydration (Hydrogel).

Training. Mice first learned to associate visual stimuli with water reward through passive instrumental conditioning. For naïve mice to learn this association, water reward was delivered 0.7s after the onset of a visual stimulus (See “Visual stimuli”, below). Following reward consumption, mice then had to withhold from licking for a mandatory period of time (exponentially distributed intervals from 0.5-6s, randomly selected per trial) in order for visual stimuli to appear on subsequent trials. Lick times were measured with custom built contactless lick detectors (Williams et al., 2018). Typically within 3 – 7 days of training, mice began licking shortly after stimulus onset and prior to reward delivery (anticipatory licking), indicating behavioral responses to the onset of the visual stimulus. Mice were then transitioned to an active paradigm where they only received rewards contingent upon licking during the stimulus presentation (typically 1 s long). On 20% of trials, 0% contrast stimuli were presented in order to measure the probability of licking to the absence of visual stimuli (false alarms). When detection performance was above chance for 2 consecutive days, the contrast and/or size of stimuli were decreased to maintain task difficulty. The main conclusions of this study involve detection of stimuli at a single position in the binocular visual field (Extended data Fig. 1-1). Once performance

was above chance for a range of low and high contrasts on binocular trials (2 - 33% contrast), we performed acute extracellular recordings.

Behavioral metrics. Detection performance was quantified with the psychometric sensitivity index (d', Green and Swets, 1974), which was calculated as:

$$d' = Z(hit\ rate) - Z(false\ alarm\ rate)$$

where Z represents the inverse of the normal cumulative distribution (MATLAB function norminv). Response bias or criterion (c) was calculated using the formula:

$$c = -\frac{Z(hit\ rate)+Z(false\ alarm\ rate)}{2}.$$

Higher criterion indicates more conservative response bias (withholding responses).

Recordings

Surgical preparation. A small craniotomy (100-400 microns) was opened over binocular V1 during isoflurane anesthesia. Mice were allowed ≥3 hours of recovery before awake acute recordings. There was no difference in behavioral performance in WT mice during recordings (d': 1.7 ± 0.5) versus the previous day (1.7 ± 0.2, *p = 0.6,* signed rank test). To remove any potential effect of anesthesia or surgery on perceptual performance in ASD mice, craniotomies were performed 12-24 hours prior to recordings to ensure equally robust behavioral performance during recordings (d': 1.7 ± 0.2 versus 1.5 ± 0.3, *p = 0.4*). For both ASD and WT anesthetized recordings, mice were given a combination of sedative chlorprothixene (0.1 mg/kg) and isoflurane (0.5-1%), as in our previous studies (Haider et al., 2016).

Electrophysiology. Single shank linear 32 site silicon probes (Neuronexus, A1x32) were used to record neural activity across cortical layers. The electrode was typically advanced to 1000 microns below the dura, and the site was covered in sterile artificial cerebrospinal fluid (aCSF). Recordings typically lasted 90 minutes, whereupon the probe was removed and the site cleaned with sterile aCSF and covered with polymer (Kwikcast). Typically we were able to record 3 consecutive days from the same craniotomy.

Visual stimuli. During behavior, mice detected Gabor gratings (0.05 - 0.1 cycles/°, σ = 10 - 20°, horizontal orientation, phase randomized per trial). Low contrast (5%) task-irrelevant bars (9˚ wide, 0.1s duration, inter-stimulus interval of 0.3s, vertical orientation) were also presented during the inter-trial intervals to facilitate receptive field mapping; these faint bars did not affect behavioral performance and they are not analyzed here. After task completion, 100% contrast bars (9˚ wide, 0.1s duration, inter-stimulus interval of 0.3s, vertical orientation, 100% contrast) were presented across the visual field to map the receptive field. These same bars were used to measure visual responses in awake mice not performing the behavioral task, and also during anesthetized experiments. The bar at the center of the receptive field and the adjacent ±1 bars were used in all subsequent analyses.

Eye Tracking. We recorded the animal's pupil during awake recordings. A high-speed camera (Imaging source DMK 21Bu04.H) with a zoom lens (Navitar 7000) and infrared filter (Mightex, 092/52x0.75) was placed ~22 cm from the animal's right eye. A near-infrared LED (Mightex, SLS-02008-A) illuminated the eye. Video files were acquired and processed using the Image Acquisition Toolbox in MATLAB with custom code. 1 mm corresponded to ~74 pixels on each frame.

Electroretinography. We tested retinal function using full-field flash electroretinography (ERG) as previously described (Mees et al., 2019). Briefly, after overnight dark-adaptation, we anesthetized mice (ketamine 60 mg/kg/, xylazine 7.5 mg/kg) under dim red light, anesthetized corneas with tetracaine (0.5%; Alcon) and dilated pupils with tropicamide (1%; Sandoz). Binocular retinal responses were measured via gold-loop corneal electrodes, with platinum needle electrodes serving as reference and ground in the cheeks and tail,

respectively. Testing consisted of 6 scotopic flashes (-4.86 – 2.5 log cd*s/m^2), followed by 10 minutes of light adaption (30 cd/m^2) and 3 photopic flashes (-0.2 – 1.4 log cd*s/m^2). Responses were differentially amplified (1-1500 Hz, 250 ms, 2 kHz) and stored (UTAS BigShot). We measured amplitude and implicit time for a and b waves (Penn and Hagins, 1969) and averaged the traces from right and left eyes for statistical analysis.

Analysis

Spike sorting. Electrical signals were acquired through a Cereplex Direct (Blackrock Microsystems). Raw neural signals were acquired at 30 kHz, and single unit activity was isolated with a semi-automated sorting algorithm (Rossant et al., 2016), as detailed in our previous studies (Speed et al., 2019). We classified single units as fast-spiking (FS, waveform peak-to-trough < 0.57ms) and regular spiking (RS, peak-to-trough > 0.57 ms) based on their waveform widths (Extended data Fig. 2-1). FS neurons in mice are predominantly paravalbumin (PV) positive inhibitory neurons, while >85% of RS neurons are putative excitatory neurons (see Speed et al., 2019).

LFP analysis. Local field potentials were band pass filtered at 0.3-200Hz. Layers were identified via current source density analysis (Niell and Stryker, 2008; Speed et al., 2019) and laminar LFP responses were calculated by taking the average across channels spanning particular layers. We analyzed the residual LFP power in hit and miss trials in the low frequency band (2-20 Hz). We calculated the residual LFP power by fitting the entire power spectrum with a single exponential that excluded the bandwidth of interest. In this bandwidth, residual LFP power is the difference between the measured power and power of the fit, normalized by the fit (Saleem et al., 2017; Speed et al., 2019).

LFP-behavior correlations. Reaction times was split into quartiles within each recording. The average residual power or stimulus-evoked spiking activity was then averaged for each quartile. A linear regression model was then fit to the data to determine if there was a correlation between neural activity and reaction time. Error bars were obtained by bootstrap resampling and repeating the fitting procedure 50 times.

Classifier. A support vector machine (SVM) classifier was constructed to predict trial outcome based on low frequency residual LFP power, as detailed elsewhere (Speed et al., 2019). The classifier was trained by randomly selecting 100 trials, and then a randomly sampled 100 trial test set was used to predict behavioral outcome (WT: hit trials = 533, miss trials = 211; ASD: hit trials=1402, miss trials = 423). This procedure was repeated 50 times to obtain error bars (±SD) for classification accuracy.

Pupil analysis. Raw video frames were cropped to isolate the eye and pupil. Frames were smoothed with a 2-D Gaussian filter. Based on pixel intensity, the pupil was identified and a least-squares error 2D ellipse was fit to the contours. The pupil area was determined by the amount of pixels in the ellipse. ∆Pupil area was calculated as the percent deviation from the mean

$$\Delta \text{ Pupil area} = [\frac{(A-\bar{A})*100}{\bar{A}}],$$

where A is the area in pixels and $\bar{A}$ is the average area across all frames. Similarly, the change in pupil position (azimuth) was calculated by subtracting the average position across all frames.

Stimulus-evoked analysis. Visually-evoked firing rates were calculated as the difference between pre-stimulus activity (0.1 s preceding the stimulus onset) and post-stimulus activity (anesthetized: 0 – 0.25 s; awake, no task: 0 – 0.125 s; awake, grating responses during task: 0 – 0.2 s). These windows were chosen based upon the duration of the LFP responses in each condition (Extended data Fig. 2-1). Violin plots of individual data points in all figures show 95% of the data range (±2.5% of range clipped for display). All statistics used full data ranges.

Experimental design and statistical analysis

Our experimental design centered on measuring neural activity and behavior during identical sensory conditions, and comparing these across ASD and WT mice matched in age, sex, recording region, and methods. Experimenters were not blinded to the group identity of each subject, but this was not required for performing identical measurements of behavioral performance or electrophysiology. We performed these studies in comparable numbers of subjects and experiments across groups. Throughout this paper, unpaired comparisons utilized Wilcoxon rank sum tests (tails specified) or sign tests (for differences from scalar values), and paired comparisons utilized Wilcoxon signed rank tests, unless otherwise noted.

Data availability

All data structures and code that generated each figure are available upon reasonable request.

Author contributions

J.D.R., H.A., A.S. performed behavioral experiments; J.D.R., A.S. performed electrophysiological experiments; C.M. performed ERG experiments and data analysis with M.P.; J.D.R., A.S., B.H. performed data analysis; J.D.R. and B.H. wrote the manuscript with feedback from all authors.

Acknowledgements

J.D.R. was funded by a Goizueta Foundation fellowship and Alfred P. Sloan Foundation's Minority Ph.D. (MPHD) Program Fellowship. B.H. was funded by the GT Neural Engineering center (1241384), the Whitehall Foundation, the Sloan Foundation, NIH NINDS (NS107968), NIH BRAIN Initiative (NS109978), and the Simons Foundation Autism Research Initiative (SFARI). M.P. was funded by Department of Veterans Affairs Rehabilitation Research and Development Service Merit Award (I01RX002615) and Senior Research Career Scientist Award (IK6RX003134).

References

Antoine MW, Langberg T, Schnepel P, Feldman DE (2019) Increased Excitation-Inhibition Ratio Stabilizes Synapse and Circuit Excitability in Four Autism Mouse Models. Neuron 101:648-661 e644.

Arking DE, Cutler DJ, Brune CW, Teslovich TM, West K, Ikeda M, Rea A, Guy M, Lin S, Cook EH, Chakravarti A (2008) A common genetic variant in the neurexin superfamily member CNTNAP2 increases familial risk of autism. Am J Hum Genet 82:160-164.

Bertone A, Mottron L, Jelenic P, Faubert J (2005) Enhanced and diminished visuo-spatial information processing in autism depends on stimulus complexity. Brain 128:2430-2441.

Burgess CP, Lak A, Steinmetz NA, Zatka-Haas P, Bai Reddy C, Jacobs EAK, Linden JF, Paton JJ, Ranson A, Schroder S, Soares S, Wells MJ, Wool LE, Harris KD, Carandini M (2017) High-Yield Methods for Accurate Two-Alternative Visual Psychophysics in Head-Fixed Mice. Cell Rep 20:2513-2524.

Douglas RJ, Martin KA (2004) Neuronal circuits of the neocortex. Annual review of neuroscience 27:419-451.

Einstein MC, Polack PO, Tran DT, Golshani P (2017) Visually Evoked 3-5 Hz Membrane Potential Oscillations Reduce the Responsiveness of Visual Cortex Neurons in Awake Behaving Mice. J Neurosci 37:5084-5098.

Estes A, Zwaigenbaum L, Gu H, St John T, Paterson S, Elison JT, Hazlett H, Botteron K, Dager SR, Schultz RT, Kostopoulos P, Evans A, Dawson G, Eliason J, Alvarez S, Piven J, network I (2015) Behavioral, cognitive, and adaptive development in infants with autism spectrum disorder in the first 2 years of life. J Neurodev Disord 7:24.

Ferraro FR (2016) No evidence of reaction time slowing in autism spectrum disorder. Autism : the international journal of research and practice 20:116-122.

Glickfeld LL, Andermann ML, Bonin V, Reid RC (2013) Cortico-cortical projections in mouse visual cortex are functionally target specific. Nat Neurosci 16:219-226.

Goel A, Cantu DA, Guilfoyle J, Chaudhari GR, Newadkar A, Todisco B, de Alba D, Kourdougli N, Schmitt LM, Pedapati E, Erickson CA, Portera-Cailliau C (2018) Impaired perceptual learning in a mouse model of Fragile X syndrome is mediated by parvalbumin neuron dysfunction and is reversible. Nat Neurosci 21:1404-1411.

Green DM, Swets JA (1974) Signal detection theory and psychophysics. Huntington, N.Y.,: R. E. Krieger Pub. Co.

Haider B, Hausser M, Carandini M (2013) Inhibition dominates sensory responses in the awake cortex. Nature 493:97-+.

Haider B, Schulz DP, Hausser M, Carandini M (2016) Millisecond Coupling of Local Field Potentials to Synaptic Currents in the Awake Visual Cortex. Neuron 90:35-42.

Isaacson JS, Scanziani M (2011) How inhibition shapes cortical activity. Neuron 72:231-243.

Karalunas SL, Geurts HM, Konrad K, Bender S, Nigg JT (2014) Annual research review: Reaction time variability in ADHD and autism spectrum disorders: measurement and mechanisms of a proposed trans-diagnostic phenotype. Journal of child psychology and psychiatry, and allied disciplines 55:685-710.

Lazaro MT et al. (2019) Reduced Prefrontal Synaptic Connectivity and Disturbed Oscillatory Population Dynamics in the CNTNAP2 Model of Autism. Cell reports 27:2567-2578 e2566.

McGinley MJ, Vinck M, Reimer J, Batista-Brito R, Zagha E, Cadwell CR, Tolias AS, Cardin JA, McCormick DA (2015) Waking State: Rapid Variations Modulate Neural and Behavioral Responses. Neuron 87:1143-1161.

Mees LM, Coulter MM, Chrenek MA, Motz CT, Landis EG, Boatright JH, Pardue MT (2019) Low-Intensity Exercise in Mice Is Sufficient to Protect Retinal Function During Light-Induced Retinal Degeneration. Invest Ophthalmol Vis Sci 60:1328-1335.

Nandy A, Nassi JJ, Jadi MP, Reynolds J (2019) Optogenetically induced low-frequency correlations impair perception. eLife 8.

Nelson SB, Valakh V (2015) Excitatory/Inhibitory Balance and Circuit Homeostasis in Autism Spectrum Disorders. Neuron 87:684-698.

Niell CM, Stryker MP (2008) Highly selective receptive fields in mouse visual cortex. J Neurosci 28:7520-7536.

Penagarikano O, Abrahams BS, Herman EI, Winden KD, Gdalyahu A, Dong H, Sonnenblick LI, Gruver R, Almajano J, Bragin A, Golshani P, Trachtenberg JT, Peles E, Geschwind DH (2011) Absence of CNTNAP2 leads to epilepsy, neuronal migration abnormalities, and core autism-related deficits. Cell 147:235-246.

Penn RD, Hagins WA (1969) Signal transmission along retinal rods and the origin of the electroretinographic a-wave. Nature 223:201-204.

Priebe NJ, Ferster D (2012) Mechanisms of neuronal computation in mammalian visual cortex. Neuron 75:194-208.

Robertson CE, Baron-Cohen S (2017) Sensory perception in autism. Nat Rev Neurosci 18:671-684.

Robertson CE, Thomas C, Kravitz DJ, Wallace GL, Baron-Cohen S, Martin A, Baker CI (2014) Global motion perception deficits in autism are reflected as early as primary visual cortex. Brain 137:2588-2599.

Rossant C, Kadir SN, Goodman DF, Schulman J, Hunter ML, Saleem AB, Grosmark A, Belluscio M, Denfield GH, Ecker AS, Tolias AS, Solomon S, Buzsaki G, Carandini M, Harris KD (2016) Spike sorting for large, dense electrode arrays. Nat Neurosci 19:634-641.

Rubenstein JL, Merzenich MM (2003) Model of autism: increased ratio of excitation/inhibition in key neural systems. Genes Brain Behav 2:255-267.

Saleem AB, Lien AD, Krumin M, Haider B, Roson MR, Ayaz A, Reinhold K, Busse L, Carandini M, Harris KD (2017) Subcortical Source and Modulation of the Narrowband Gamma Oscillation in Mouse Visual Cortex. Neuron 93:315-322.

Scott R, Sanchez-Aguilera A, van Elst K, Lim L, Dehorter N, Bae SE, Bartolini G, Peles E, Kas MJH, Bruining H, Marin O (2019) Loss of Cntnap2 Causes Axonal Excitability Deficits, Developmental Delay in Cortical Myelination, and Abnormal Stereotyped Motor Behavior. Cerebral cortex 29:586-597.

Sohal VS, Rubenstein JLR (2019) Excitation-inhibition balance as a framework for investigating mechanisms in neuropsychiatric disorders. Mol Psychiatry.

Speed A, Del Rosario J, Burgess CP, Haider B (2019) Cortical State Fluctuations across Layers of V1 during Visual Spatial Perception. Cell reports 26:2868-2874 e2863.

Sutherland A, Crewther DP (2010) Magnocellular visual evoked potential delay with high autism spectrum quotient yields a neural mechanism for altered perception. Brain 133:2089-2097.

Tavassoli T, Latham K, Bach M, Dakin SC, Baron-Cohen S (2011) Psychophysical measures of visual acuity in autism spectrum conditions. Vision research 51:1778-1780.

Tavassoli T, Miller LJ, Schoen SA, Nielsen DM, Baron-Cohen S (2014) Sensory over-responsivity in adults with autism spectrum conditions. Autism : the international journal of research and practice 18:428-432.

Tomchek SD, Dunn W (2007) Sensory processing in children with and without autism: a comparative study using the short sensory profile. The American journal of occupational therapy : official publication of the American Occupational Therapy Association 61:190-200.

van der Geest JN, Kemner C, Camfferman G, Verbaten MN, van Engeland H (2001) Eye movements, visual attention, and autism: a saccadic reaction time study using the gap and overlap paradigm. Biol Psychiatry 50:614-619.

Velmeshev D, Schirmer L, Jung D, Haeussler M, Perez Y, Mayer S, Bhaduri A, Goyal N, Rowitch DH, Kriegstein AR (2019) Single-cell genomics identifies cell type–specific molecular changes in autism. Science 364:685-689.

Williams B, Speed A, Haider B (2018) A novel device for real-time measurement and manipulation of licking behavior in head-fixed mice. J Neurophysiol 120:2975-2987.

Diminished cortical excitation during perceptual impairments in a mouse model of autism

Joseph Del Rosario, Anderson Speed, Hayley Arrowood, Cara Motz, Machelle Pardue, Bilal Haider

Extended Data

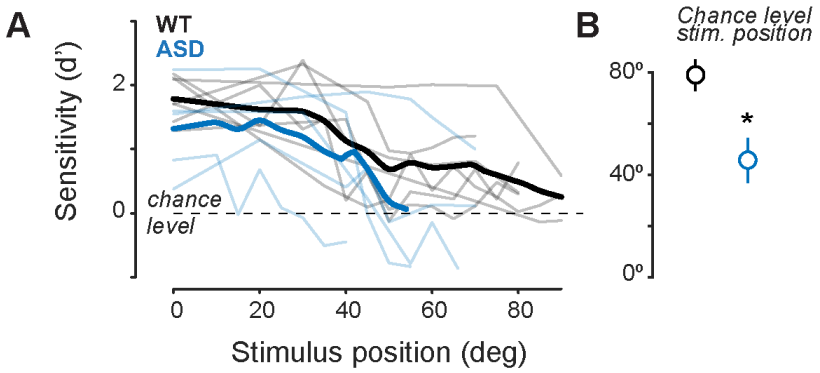

Figure 1-1. Monocular visual detection performance is reduced in ASD mice

a. Detection sensitivity (d') versus stimulus position. Vertical meridian at 0˚, in the binocular visual field. Thick lines show mean across individual mice. Data show detection performance averaged across high contrasts (>65%).

b. Detection sensitivity of WT mice drops to chance level at significantly farther eccentricity (72 ± 2˚, n = 7 mice, n = 7 mice) versus ASD mice (49 ± 4˚, n = 5 mice, *p<0.01* single tail rank sum). Mean ± SEM.

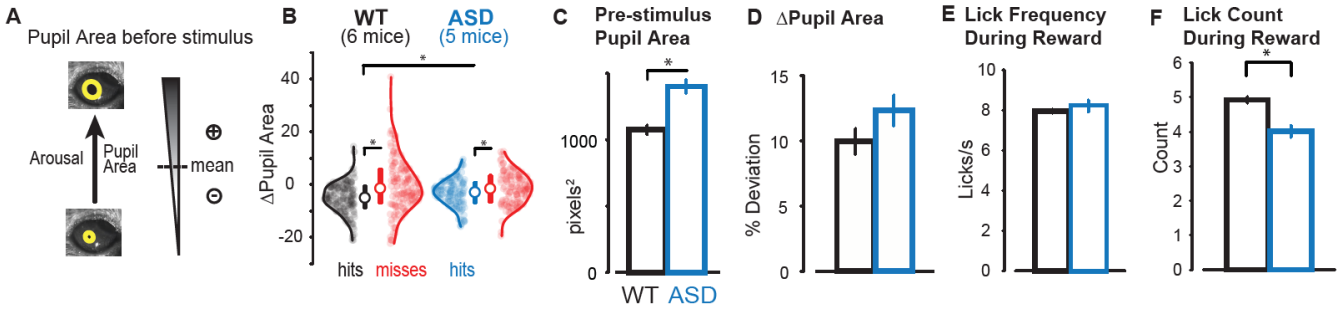

Figure 1-2. Arousal and motor activity do not explain perceptual impairments

- **a.** Pupil area was measured during each trial. Larger positive deviation of pupil area from mean indicates higher arousal.
- **b.** ΔPupil area preceding stimulus onset on Hit trials was significantly smaller than Miss trials in both WT (Hits: -5.2 ± 0.5%; Misses: -0.5 ± 0.8%; n = 190 sessions in 6 mice; mean ± SEM throughout the figure; *p<0.01*, rank sum test) and ASD mice (Hits: -3.2 ± 0.5%; Misses: -1.5 ± 0.6%; n = 138 sessions in 5 mice; *p<0.01,* rank sum test). ΔPupil area preceding Hits was significantly smaller in WT versus ASD mice (*p<0.01*, rank sum test), but not for Misses (*p=0.65*, rank sum test). ΔPupil area was calculated as the frame-by-frame percent deviation from the mean pupil area of the whole recording session (see Methods). Median ± IQR is plotted inside the distributions.
- **c.** Overall mean pupil area was larger in ASD versus WT mice (WT: 1075 ± 35 pixels^2, ASD = 1402 ± 51 pixels^2; *p<0.01,* rank sum test).
- **d.** ΔPupil area during reward consumption was not significantly different between WT (10.0 ± 1.0%) and ASD mice (12.3 ± 1.2%; *p=0.57*, rank sum test).
- **e.** Lick frequency during reward was not significantly different between WT (8.0 ± 0.1) and ASD mice (8.2 ± 0.3; *p=0.12,* rank sum test).
- **f.** Lick count during reward bouts was significantly smaller in ASD mice (4.0 ± 0.2) compared to WT mice (5.0 ± 0.1, *p < 0.01*, rank sum test). Note that this is a difference of just 1 lick / bout.

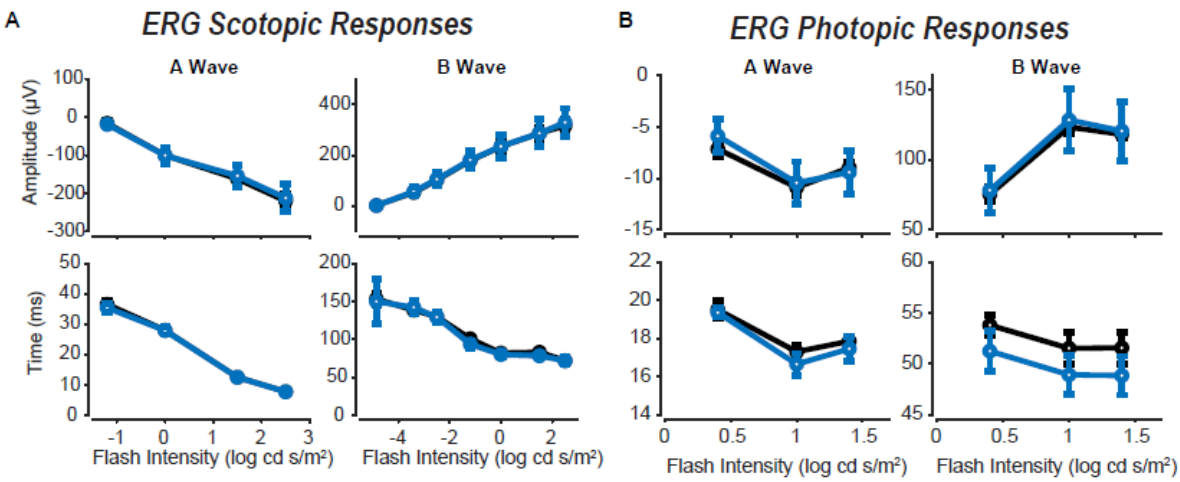

Figure 1-3. Retinal responses do not explain perceptual differences

a. Electroretinography (ERG) of scotopic responses (dark adapted; rod-dominated) as measured by the peak amplitude (top rows) and implicit time of the peak amplitude (bottom rows) for the initial negative deflection (a Wave, left) and the subsequent positive deflection (b Wave, right), which corresponds to the hyperpolarization of photoreceptor cells and depolarization of bipolar cells (Penn and Hagins, 1969). Neither the peak amplitude (a wave: *p=0.94*; b wave: *p=0.94*, n = 4 WT and 4 ASD mice) nor implicit time (a wave: *p=1*; b wave: *p=0.52*) were significantly different between WT and ASD mice. Mean ± SEM is plotted throughout the figure. See (Mees et al., 2019) for detailed description of ERG Methods.

b. Same as a, but for photopic responses (light adapted; cone-isolating). Neither the peak amplitude (a wave: *p=0.99*; b wave: *p=0.58*, 4 WT and 4 ASD mice) nor implicit time (a wave: *p=0.62*; b wave: *p=0.08*) were significantly different between WT and ASD mice.

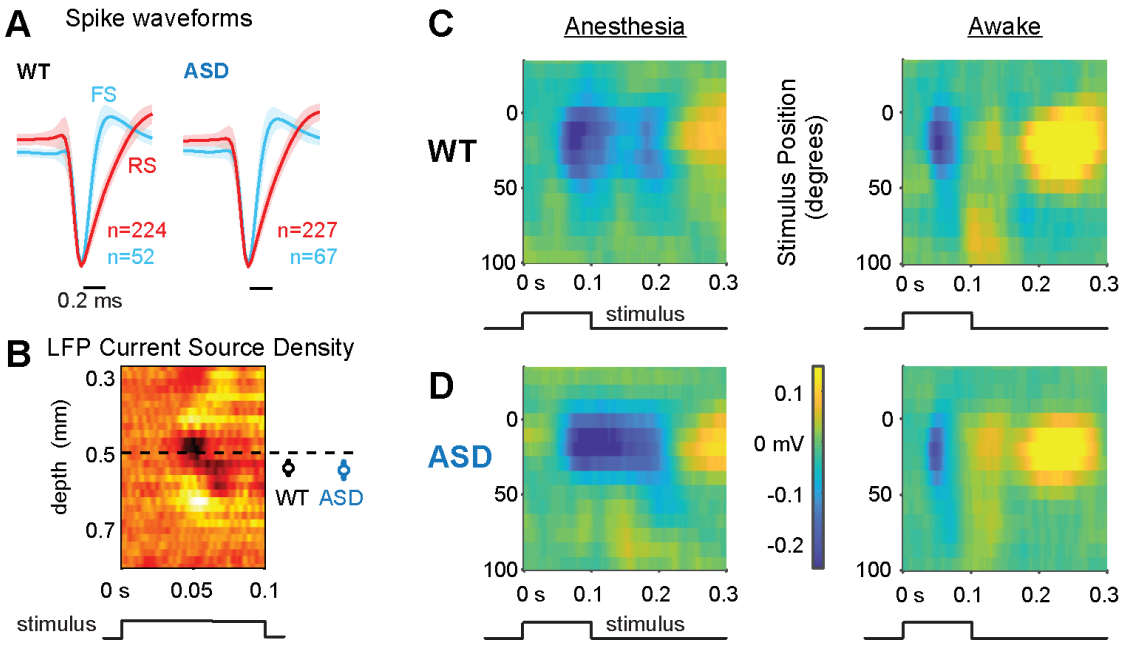

Figure 2-1. Spike waveforms, laminar estimates, receptive field locations, and response durations are similar across WT and ASD recordings

a. Population spike waveforms of fast-spiking (FS) putative inhibitory neurons and regular spiking (RS) putative excitatory neurons in WT and ASD mice (mean ± SEM). Individual waveforms normalized to maximum negative deflection before averaging.

b. Left, Example current source density (CSD) heatmap showing response to high contrast bar onset in best spatial location. Rows indicate LFP sampled across cortical layers, stimulus time course at bottom. Dark colors identify earliest and largest current sink, presumed to be layer 4 (L4). Right, population estimates of L4 from CSD are similar across WT (0.51 ± 0.02 mm, mean ± SEM, n = 23) and ASD mice (0.51 ± 0.02 mm, n = 28).

c. Spatial tuning of local field potential (LFP) responses in V1 of WT mice recorded during anesthesia (left; n = 13 recordings, 4 mice) and wakefulness (right; n = 10 recordings, 4 mice). Ordinate indicates stimulus (bar) position (in azimuth, vertical meridian at 0˚), abscissa shows time course. Note that both WT and ASD spatial tuning peaks within the central 20˚ of the visual field, in the binocular zone where grating stimuli appeared (centered at 0˚).

d. Same as c, for ASD mice during anesthesia (left, n=18 recordings, 4 mice) or wakefulness (right, n = 10 recordings, 4 mice). Note that state-dependent amplitude and time course of LFP spatial tuning is similar across ASD and WT recordings.

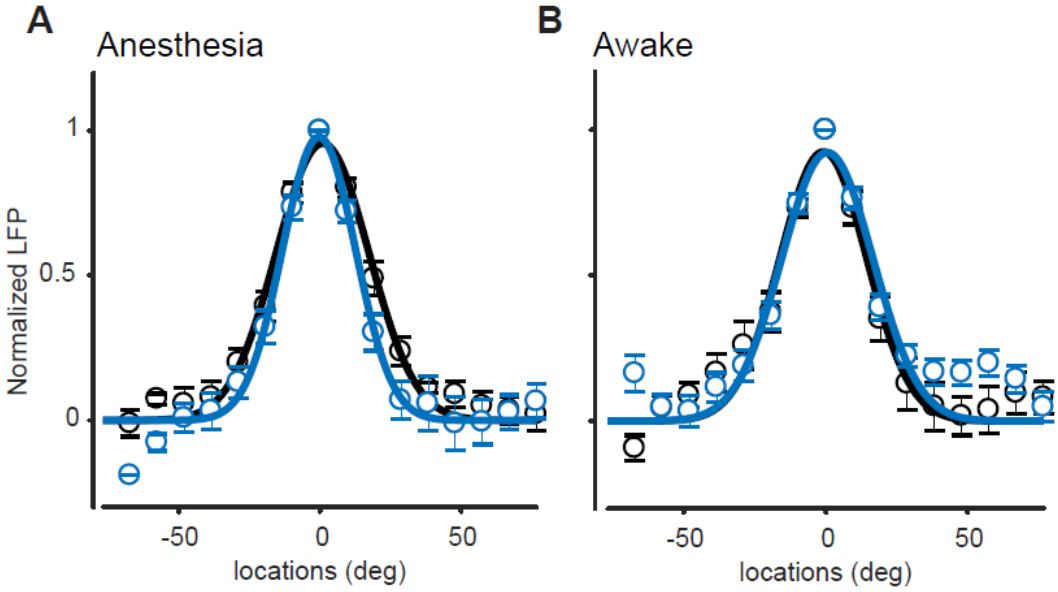

Figure 2-2. Receptive field spatial tuning is similar between ASD and WT mice

a. Average LFP receptive field spatial tuning for anesthetized recordings. Responses were normalized by maximum LFP response, and then responses averaged for all other bar positions at this time of maximum response. Response curves were then aligned at 0 (spatial position eliciting maximum response). Receptive field size (half-width of Gaussian fit) was not significantly different between WT (18 ± 5˚, mean ± SD) and ASD (15 ± 4˚) mice (*p=0.29,* rank sum test).

b. Same as in a, except for awake recordings. WT (19 ± 14˚) and ASD (18 ± 9˚) half widths are not significantly different (*p=0.96,* rank sum test)

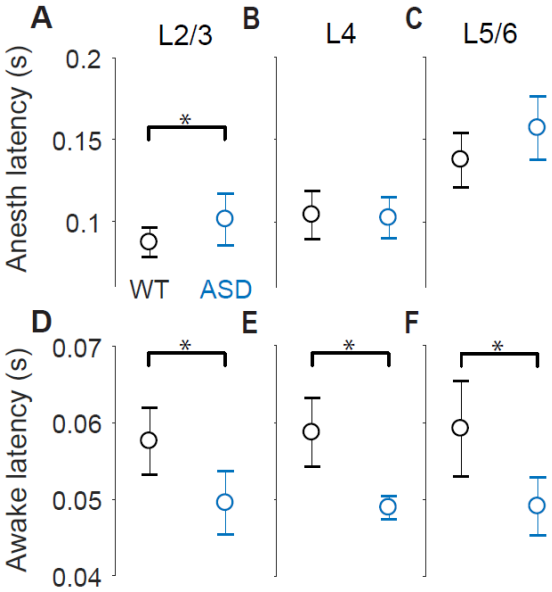

Figure 2-3. Laminar LFP response latencies across brain states in WT and ASD mice

a-c. LFP peak response latency to best bar (100% contrast, center of receptive field) during anesthesia in WT and ASD mice. Mean ± SEM throughout figure.
L2/3: WT = 87 ± 9 ms, ASD = 101 ± 16 ms (*p=0.04*, rank sum test).
L4: WT = 104 ± 15 ms, ASD = 102 ± 12 ms (*p=0.42*, rank sum test).
L5/6: WT = 138 ± 17ms, ASD = 157 ± 19 ms (*p=0.6*, rank sum test).

d-f. Same as a-c, but during wakefulness. LFP response latency is significantly faster in ASD mice across all layers.
L2/3: WT = 58 ± 42 ms, ASD=50 ± 4 ms (*p=0.05*, rank sum test).
L4: WT = 59 ± 4 ms, ASD = 49 ± 1 ms (*p=0.01*, rank sum test).
L5/6: WT = 59 ± 6 ms, ASD = 49 ± 4 ms (*p<0.01*, rank sum test).

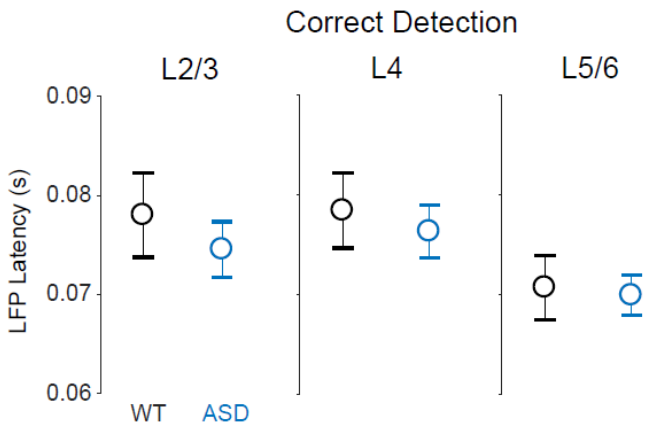

Figure 2-4. LFP latencies to detected stimuli do not explain perceptual differences

There were no significant differences in LFP response latency across layers to gratings successfully detected for rewards in WT versus ASD mice. Response latency was calculated as the time the local field potential (LFP) had the greatest negative deflection during the grating presentation on Hit trials. Mean ± SEM throughout the figure.

L2/3: WT=78 ± 4 ms (n = 533 trials, 7 recordings, 3 mice), ASD=75 ± 3 ms (n = 1402 trials, 15 recordings, 3 mice; *p=0.65, rank sum test*).

L4: WT=78 ± 4 ms, ASD=76 ± 3 ms; *p=0.8*.

L5/6: WT=71 ± 3 ms, ASD=70 ± 2 ms; *p=0.7*.

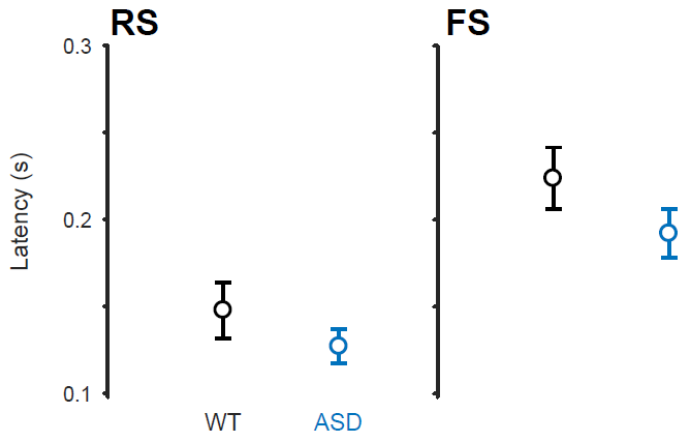

Figure 2-5. Single unit response latencies not explain perceptual differences.

Left, Regular Spiking (RS) putative excitatory neuron response latencies, measured as time of maximum firing rate during grating presentation on Hit trials. WT = 148 ± 16 ms (mean ± SEM throughout the figure, n = 49 neurons); ASD = 127 ± 10 ms (n = 103 neurons; *p=0.41*, rank sum test). Responses aggregated across layers.

Right, Fast Spiking (FS) putative inhibitory neuron response latencies: WT = 223 ± 19 ms (n = 20 neurons); ASD=192 ± 14 ms (n = 38 neurons; *p=0.17*, rank sum test).

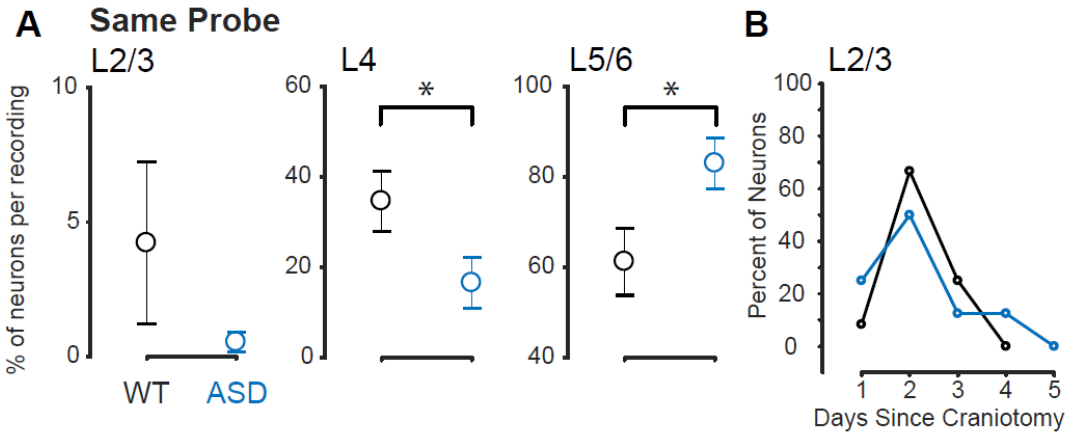

Figure 3-1. Reduced activity of L2/3 neurons in ASD mice is not due to differences in recording quality

a. Percentage of L2/3 neurons recorded with the same silicon probe in ASD versus WT experiments. On average the % yield of L2/3 neurons was not significantly different across WT and ASD recordings (WT: 4.2 ± 3.0%, ASD: 0.5 ± 0.4%, mean ± SEM throughout the figure, n=15 recordings and n = 24 recordings *p=0.13*, one-tail rank sum test). In these same experiments, there were more L4 neurons isolated in WT versus ASD recordings (WT: 34.6 ± 6.7%, ASD: 16.5 ± 5.6%, *p<0.05,* one-tail rank sum test) but more neurons isolated from L5/6 in ASD versus WT mice (WT: 61.2 ± 7.42, ASD: 83.0 ± 5.6, *p<0.05,* one-tail rank sum test).

b. Aggregated across all recordings, day 2 of recording in the same craniotomy yields the most L2/3 neurons in both WT (66.7%) and ASD (50%) mice. This indicates that the low activity and isolation of L2/3 neurons in ASD mice was not due to poorer recording quality across the same number of recording sessions as WT mice.

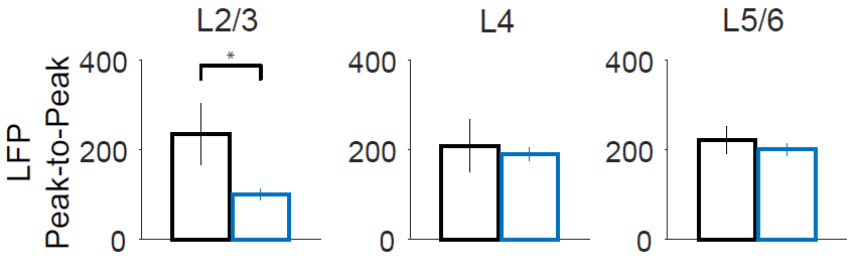

Figure 3-2. LFP amplitude range is reduced specifically in L2/3 in ASD mice

Peak-to-peak stimulus-evoked LFP in L2/3 on Hit trials is significantly smaller in ASD mice (98 ± 12 μV, mean ± SEM throughout the figure, n = 1402 trials, 15 recordings, 3 mice) versus WT mice (235 ± 68 μV, n = 533 trials, 7 recordings, 3 mice; $p<0.01$, single-tailed rank sum tests for all).

No other layer was affected (L4: WT=207 ± 58 μV, ASD=189 ± 15 μV, $p=0.31$; L5/6: WT=216 ± 30 μV, ASD=190 ± 12 μV; $p=0.26$.)